Full-Color Delayed Fluorescence Materials Based on Wedge-Shaped Phthalonitriles and Dicyanopyrazines: Systematic Design, Tunable Photophysical Properties, and OLED Performance

*In Seob Park, Sae Youn Lee, Chihaya Adachi, and Takuma Yasuda**

Purely organic light-emitting materials, which can harvest both singlet and triplet excited states to offer high electron-to-photon conversion efficiencies, are essential for the realization of high-performance organic light-emitting diodes (OLEDs) without using precious metal elements. Donor–acceptor architectures with an intramolecular charge-transfer excited state have been proved to be a promising system for achieving these requirements through a mechanism of thermally activated delayed fluorescence (TADF). Here, luminescent wedge-shaped molecules, which comprise a central phthalonitrile or 2,3-dicyanopyrazine acceptor core coupled with various donor units, are reported as TADF emitters. This set of materials allows systematic fine-tuning of the band gap and exhibits TADF emissions that cover the entire visible range from blue to red. Full-color TADF-OLEDs with high maximum external electroluminescence quantum efficiencies of up to 18.9% have been demonstrated by using these phthalonitrile and 2,3-dicyanopyrazine-based TADF emitters.

1. Introduction

Organic light-emitting diodes (OLEDs) are now used in mainstream display technologies and are also being explored intensively for future lighting applications owing to their unique advantages such as the high electroluminescence (EL) efficiency, high contrast, light weight, flexibility, and low manufacturing costs.[1] In OLEDs, electrically injected holes and electrons recombine to form singlet and triplet excitons with a ratio of 1:3, according to spin statistics.[2] Therefore, internal EL quantum efficiencies (η_{int}) of OLEDs based on conventional fluorescent materials are limited to 25% as only the lowest singlet (S_1) excitons can be utilized for light emission under electrical excitations. In this case, the lowest triplet (T_1) excitons undergo a spin-forbidden transition, resulting in radiation-less deactivation. Meanwhile, precious metal-containing organometallic phosphorescent materials are capable of harvesting both S_1 and T_1 excitons for light emission.[2] This is because of the enhanced intersystem crossing (ISC) mediated by a strong spin–orbit coupling of the heavy metals such as iridium, platinum, and osmium, which results in η_{int} of up to 100%.[3] Despite their desirable EL characteristics, the rarity, high cost, and toxicity of these precious metals, as well as the poor stability of blue phosphors would hamper the widespread applications of these OLEDs in the future. As an alternative, thermally activated delayed fluorescence (TADF, **Figure 1**), which occurs by converting the excited T_1 states to emissive S_1 states via an efficient reverse intersystem crossing (RISC) using purely organic emitters, has attracted great attention in recent years.[4–9] Highly efficient TADF-OLEDs with η_{int} of nearly 100% have been successfully realized, and hence, TADF is expected to be a key technology for the next-generation OLEDs.

The major design principle for TADF molecules is to minimize the overlap between the highest occupied molecular orbital (HOMO) and the lowest unoccupied molecular orbital (LUMO) by localizing them on different moieties in a molecule, leading to a small energy gap between the excited S_1 and T_1 states (ΔE_{ST}), as a consequence of reduced electron exchange interactions.[10] Under this condition, the RISC process can be strongly accelerated. However, a weak frontier orbital overlap is a prerequisite for an efficient light emission, because a negligible spatial overlap of the wavefunctions results in the loss of transition probability according to Fermi's golden rule. Therefore, both these conditions should be met for designing novel efficient TADF molecules. Based on this design principle, various purely organic TADF emitters have been developed to date;[4–9] most of them adopt a twisted intramolecular

I. S. Park, Prof. T. Yasuda
INAMORI Frontier Research Center (IFRC)
Kyushu University
744 Motooka, Nishi-ku
Fukuoka 819-0395, Japan
E-mail: yasuda@ifrc.kyushu-u.ac.jp
I. S. Park, Dr. S. Y. Lee, Prof. C. Adachi, Prof. T. Yasuda
Department of Applied Chemistry
Graduate School of Engineering
Kyushu University
744 Motooka, Nishi-ku
Fukuoka 819-0395, Japan
Prof. C. Adachi
Center for Organic Photonics and Electronics Research (OPERA)
Kyushu University
744 Motooka, Nishi-ku
Fukuoka 819-0395, Japan

DOI: 10.1002/adfm.201505106

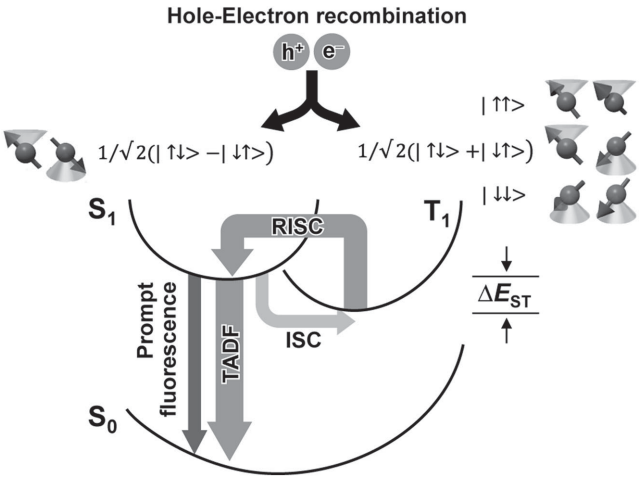

Figure 1. Schematic representation for TADF mechanism in OLEDs. Upon hole and electron recombination, 25% of the corresponding excited states are singlets, while 75% are triplets. The triplet excitons are harvested through thermally promoted $T_1 \rightarrow S_1$ RISC to emit TADF.

charge-transfer (ICT) design, in which the electron donor and acceptor units are incorporated to be orthogonal to each other. Among the reported TADF emitters, 1,2,3,5-tetrakis(carbazol-9-yl)-4,6-dicyanobenzene (4Cz-IPN)[4a] combined with an electron-withdrawing isophthalonitrile (i.e., 1,3-dicyanobenzene) with fourfold electron-donating carbazole units is one of the most efficient TADF emitters, exhibiting a maximum external EL quantum efficiency (η_{ext}) of almost 20%[4a] or even higher.[11] It has also been reported that by changing the position of cyano groups and the number of carbazole units, the emission spectra of the TADF materials can be tuned. ICT of these molecules has crucial effects on their band gap and luminescence. For the realization of full-color TADF-OLEDs, it is vital to modulate the TADF characteristics and the emission colors systematically using a versatile donor–acceptor (D–A) system.

In this work, a series of wedge-shaped donor–acceptor–donor (D–A–D) molecules (**Figure 2**), comprising a central phthalonitrile (VPN) or 2,3-dicyanopyrazine (CNP) acceptor core coupled with various donor units (i.e., 1-methylcarbazole (Cz), 9,9-dimethylacridan (Ac), and phenoxazine (Px)), are reported. π-Conjugated phenylene linkers are introduced between the donor and acceptor units to enhance the radiative decay constant of the S_1 state to some degree, meanwhile maintaining a small ΔE_{ST}. These new systems allow a systematic fine-tuning of their band gap and TADF emissions to cover the entire visible range. Full-color EL with a high η_{ext} of up to 18.9% can be achieved using wedge-shaped phthalonitrile and dicyanopyrazine derivatives as TADF emitters in OLEDs.

2. Results and Discussion

2.1. Molecular Geometric and Electronic Structures

To understand the effect of variation of the D–A–D structures on the geometric and optoelectronic properties,

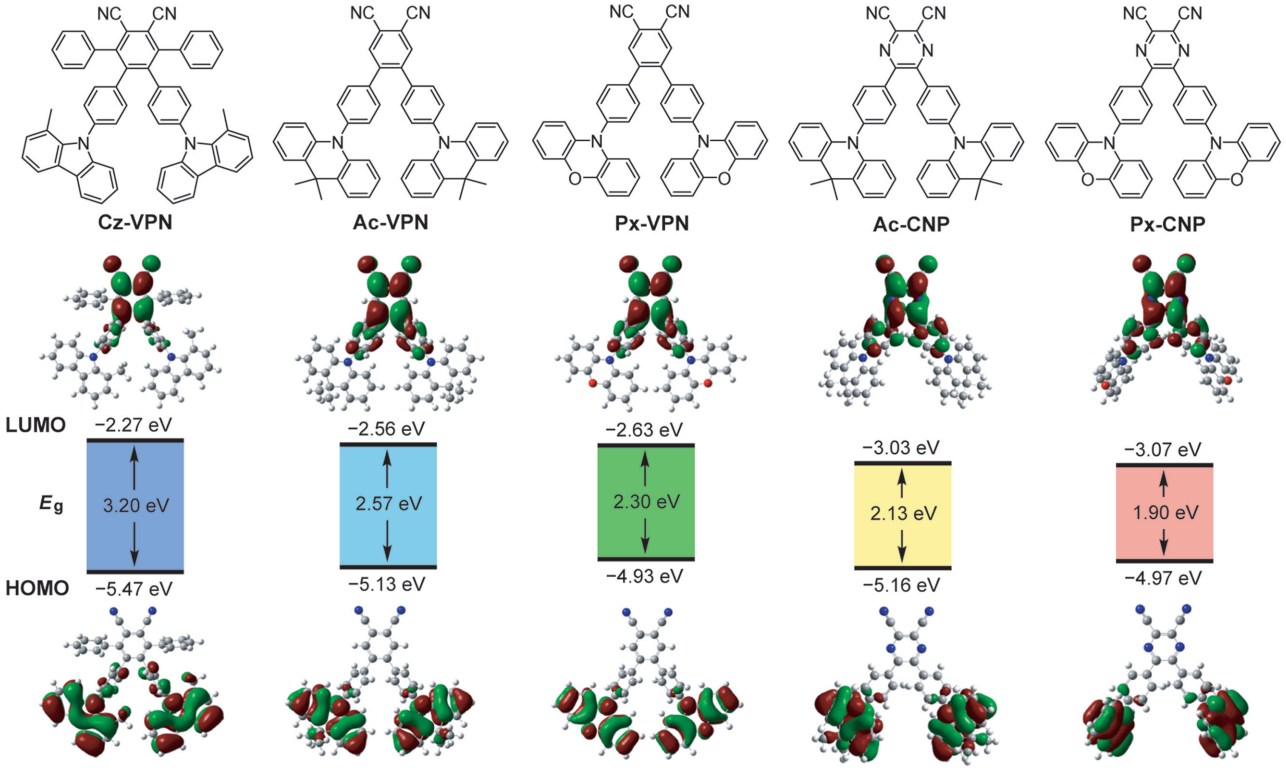

Figure 2. Molecular structures (upper), energy levels and Kohn–Sham orbitals of the HOMO and LUMO (lower) of wedge-shaped phthalonitrile and dicyanopyrazine-based TADF molecules characterized by DFT and TD-DFT calculations at the B3LYP/6-31G(d,p) level.

quantum-chemical calculations were performed on the designed phthalonitrile and dicyanopyrazine-based molecules. The calculated energy levels of the HOMO and LUMO and the respective frontier orbital distributions are presented in Figure 2. The energy levels and molecular geometries in the ground state were optimized by density functional theory (DFT) calculations. The excited S_1 and T_1 states were computed using the optimized structures with time-dependent DFT (TD-DFT) calculations. It is found that the calculated HOMO–LUMO energy gaps (E_g) can be modulated systematically from 3.2 eV (Cz-VPN) to 1.9 eV (Px-CNP) by a rational combination of donor and acceptor units. The decrease in the E_g from Cz-VPN to Px-VPN follows the increasing order of the electron-donating ability of their donor units (Cz < Ac < Px) which consequently affects their HOMO energy levels. Ac-CNP and Px-CNP containing a strong electron-withdrawing dicyanopyrazine core tend to have a lower LUMO energy and a narrower E_g than the phthalonitrile-based counterparts do. This trend indicates that the donor and acceptor strengths have a great influence on the resulting optoelectronic functionality since the HOMO–LUMO electronic transition dominates the S_1 excitation with ICT characteristics.

The HOMOs of these molecules are predominantly located on the peripheral donor units, whereas the LUMOs are distributed over the phenylene linkers as well as the central acceptor core (Figure 2). For Cz-VPN, the HOMO is extended slightly to the neighboring phenylene linkers, owing to the less steric hindrance of the Cz donor units, compared with the Ac and Px units. The clear spatial separation of the frontier orbitals of all these molecules resulted in small calculated ΔE_{ST} values of less than 0.04 eV (**Table 1**), suggesting the high potential as TADF emitters. It is also evident that, in the optimized ground-state structures, the dihedral angles between the peripheral donor units and the nearby phenylene linkers increase in the order of Cz (53°–54°) < Px (74°–77°) < Ac (87°–90°). Such highly distorted geometries of these molecules should arise from the steric effects of the hydrogen atoms and/or methyl groups at the peri-positions in the donor units, contributing to the decrease of the electron exchange energy for the ICT transitions. In contrast, the dihedral angles between the central phthalonitrile or dicyanopyrazine acceptor unit and the phenylene linkers are relatively small (51°–54° for Ac-VPN and Px-VPN; 34°–35° for Ac-CNP and Px-CNP). These results suggest that the phenylene linker has a stronger conjugation with the central acceptor core than the outermost donor units.

2.2. Synthesis

The synthetic scheme is outlined in **Scheme 1**, and the detailed synthetic procedures are described in the Experimental Section and the Supporting Information. The key intermediate **2** was synthesized from tetraphenylcyclopentadienone **1** and fumaronitrile.[12] Then, the Buchwald–Hartwig amination of **2** with 1-methylcarbazole in the presence of Pd(*t*-$Bu_3P)_2$ as a catalyst afforded Cz-VPN with a high yield. The syntheses of Ac-VPN and Px-VPN were achieved by Suzuki–Miyaura cross-coupling reactions between 4,5-dichlorophthalnitrile and the corresponding boronic esters (**5** and **7**, respectively). For the synthesis of Ac-CNP and Px-CNP, the dibromoprecursor **8** was initially prepared, and the Buchwald–Hartwig aminations with 9,9-dimethylacridan or phenoxazine were carried out. All final products were purified by temperature-gradient sublimation under vacuum after column chromatography to obtain highly pure materials, which can be used for the fabrication of OLED devices by vacuum deposition. Chemical structures of the final products were confirmed by ^1H and ^{13}C nuclear magnetic resonance (NMR) spectroscopy, matrix-assisted laser desorption ionization time-of-flight (MALDI-TOF) mass spectrometry, and elemental analysis (see the Experimental Section for details).

2.3. Photophysical Properties

The molecular orbital distributions are reflected in the photophysical properties of the phthalonitrile and dicyanopyrazine-based materials. Basic photophysical parameters have been collected from steady-state UV–vis absorption and photoluminescence (PL) spectra, and time-resolved transient PL analyses for toluene solutions and as doped thin films, and the results are summarized in Table 1. As shown in **Figure 3**, these compounds exhibit a broad and weak absorption band at longer wavelengths in the absorption spectra, which can be assigned to the ICT transitions from the peripheral donor units to the acceptor core. The ICT absorption band shifts to lower energies

Table 1. Photophysical data of phthalonitrile and dicyanopyrazine-based TADF materials.

Compound	λ_{abs} [nm] sol[a]	λ_{PL} [nm] sol[a]/film[b]	Φ_{PL}[c] [%] sol[a]/film[b]	τ_p[d] [ns]/ τ_d[d] [μs]	HOMO[e] [eV]	LUMO[f] [eV]	E_S/E_T[g] [eV]	ΔE_{ST}[h] [eV]	Calc. ΔE_{ST}[i] [eV]
Cz-VPN	292,325,339[j]	440 / 450	78 / 63	41 / 173	–6.1	–2.9	3.08 / 2.72	0.36	0.039
Ac-VPN	282,384	532 / 499	59 / 86	35 / 5.1	–5.8	–3.1	2.90 / 2.70	0.20	0.002
Px-VPN	304,406	577 / 540	42 / 77	27 / 2.3	–5.7	–3.3	2.64 / 2.56	0.08	0.015
Ac-CNP	282,342[j],436	620 / 570	20 / 67	30 / 3.3	–5.4	–3.1	2.33 / 2.24	0.09	0.003
Px-CNP	321,473	–[k] / 610	<1 / 15	21 / 1.5	–5.2	–3.2	2.45 / 2.41	0.04	0.040

[a]Measured in oxygen-free toluene solution at room temperature; [b]6 wt%-doped thin film in a host matrix (host: PPF for Cz-VPN and mCBP for others); [c]Absolute PL quantum yield evaluated using an integrating sphere under a nitrogen atmosphere; [d]PL lifetimes of prompt (τ_p) and delayed (τ_d) decay components for the 6 wt%-doped film measured using a streak camera at 300 K; [e]Determined by photoelectron yield spectroscopy in pure neat films; [f]Deduced from the HOMO and optical energy gap (E_g); [g]Singlet (E_S) and triplet (E_T) energies estimated from onset wavelengths of the emission spectra at 300 and 50 K in the doped films, respectively; [h]$\Delta E_{ST} = E_S - E_T$; [i]Calculated by TD-DFT at B3LYP/6-31G(d,p); [j]Shoulder peak; [k]Not determined.

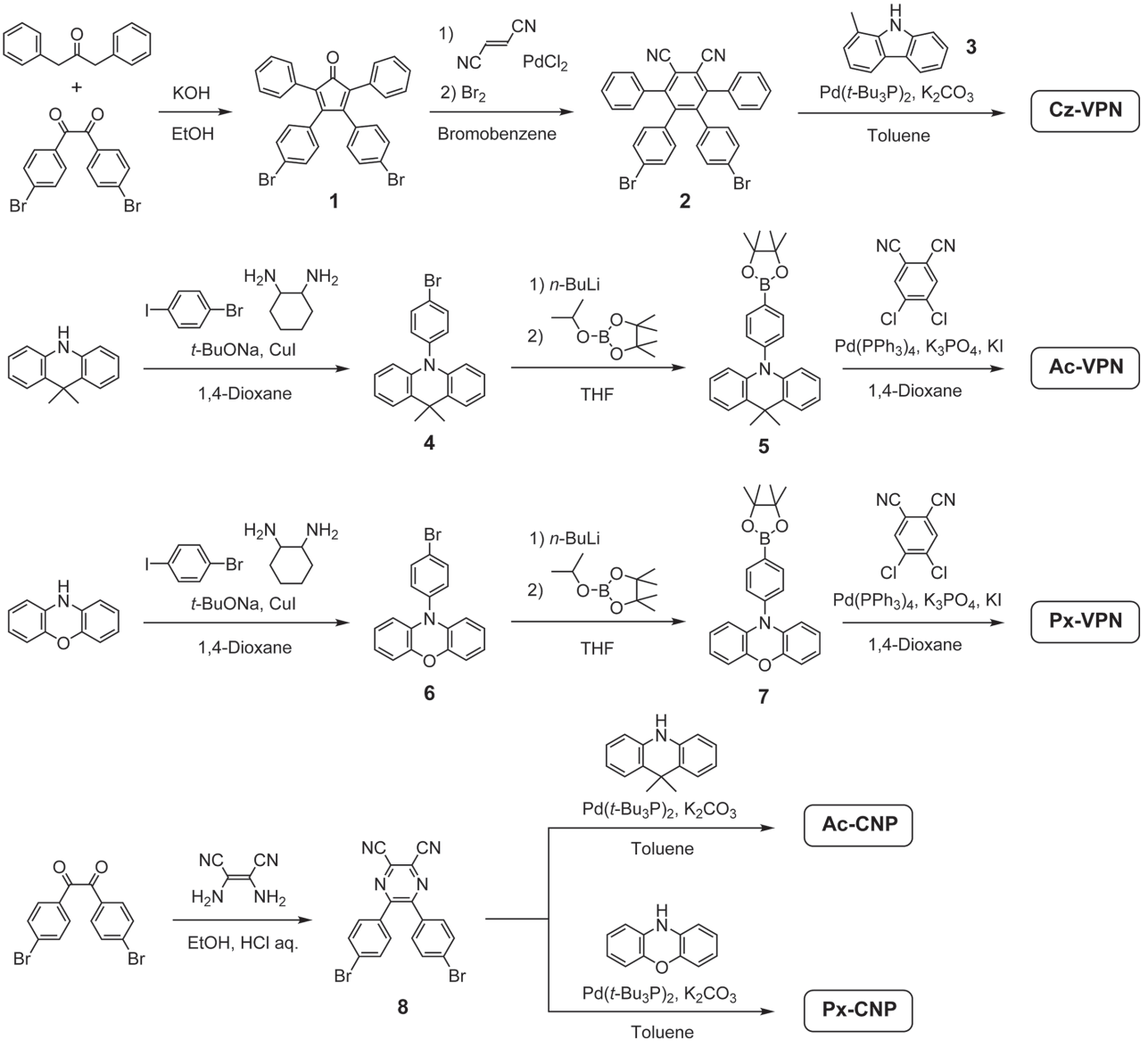

Scheme 1. Synthetic routes for phthalonitrile and dicyanopyrazine-based TADF molecules.

with increasing donor and acceptor strengths, which is well in accordance with the calculation results.

For further investigation of the photophysical and TADF properties, doped thin films of the phthalonitrile and dicyanopyrazine-based emitters in a host matrix were prepared in order to avoid concentration quenching. For the blue emitter Cz-VPN, 2,8-bis(diphenylphosphoryl)dibenzo[*b*,*d*]furan (PPF)[13] possessing a high T_1 energy (E_T) value of 3.1 eV was selected as a host to prevent the backward energy transfer from the excited Cz-VPN to the host material and to confine the T_1 excitons within the Cz-VPN molecules. For other emitters, 3,3′-bis(carbazol-9-yl)-1,1′-biphenyl (mCBP)[14] with an E_T of 2.9 eV was adopted as a suitable host material. As can be seen from **Figure 4**, the emission colors of the doped films range from blue (Cz-VPN: λ_{PL} = 450 nm) to green (Px-VPN: λ_{PL} = 540 nm), and even red (Px-CNP: λ_{PL} = 610 nm), covering the entire visible light. In contrast, Px-CNP exhibited no PL emission in dissolved states. The absolute PL quantum yields (Φ_{PL}) of these emitters in the doped films lie in the range of 63%–86%, with the exception for the red-emitting Px-CNP film (Φ_{PL} = 15%). The reason for such a low Φ_{PL} of Px-CNP may be ascribed to the energy-gap law, which suggests that the Φ_{PL} decreases as the energy gap is reduced, owing to the vibrational overlap of the ground and the excited states.[15] Thus, the experimental PL observations confirm the expected trend that the multicolor tuning of TADF can be accomplished by systematic structural variations.

We also examined the transient PL characteristics of the emitters to reveal the TADF behavior. As exemplified in **Figure 5**, the transient PL curve of the 6 wt%-Ac-VPN:mCBP doped film obviously indicated a nanosecond-order prompt decay component and a microsecond-order delayed decay component in the time range of 10 μs, which can be fitted with a biexponential

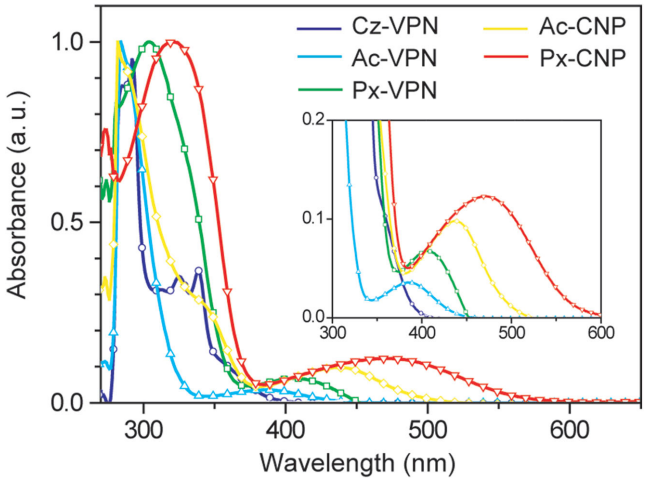

Figure 3. UV–vis absorption spectra of phthalonitrile and dicyanopyrazine-based D–A–D type molecules in toluene. The inset shows a magnified view of lower-energy ICT absorptions.

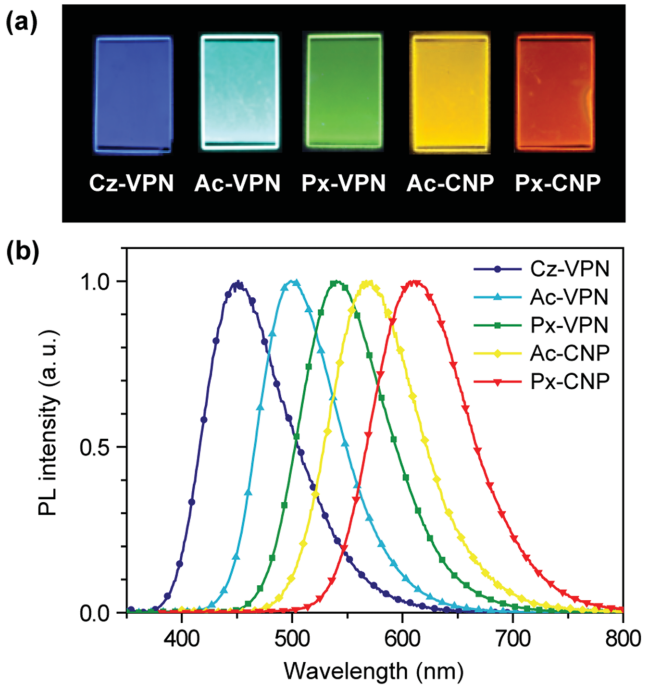

Figure 4. a) Photographs showing PL emission under UV irradiation and b) steady-state PL spectra of 6 wt%-doped thin films of the phthalonitrile and dicyanopyrazine-based emitters in a PPF or mCBP host matrix.

model. While the prompt component had a lifetime (τ_p) of 35 ns with a quantum efficiency (Φ_p) of 8%, the delayed component had a lifetime (τ_d) of 5.1 µs with an efficiency (Φ_d) of 78% at 300 K. Moreover, the delayed component is appeared with a similar spectral distribution as the prompt one; hence, the delayed emission can be ascribed to the singlet emission through RISC processes. Temperature dependence of the transient PL was also studied for the 6 wt%-Ac-VPN:mCBP doped film in the temperature range of 50–300 K (Figure 5a). Apparently, the delayed emission was intensified when temperature was increased from 50 to 300 K, demonstrating that the $T_1 \rightarrow S_1$ RISC process was enhanced by the thermal energy, which is a direct evidence of TADF. Similar temperature-dependent transient PL behavior was observed for all the phthalonitrile and dicyanopyrazine-based emitters (Supporting Information). The delayed emission lifetime of the green-emitting Px-VPN film (τ_d = 2.3 µs) is found to be much shorter than those of the blue-emitting Cz-VPN and light-blue-emitting Ac-VPN films (τ_d = 173 and 5.1 µs, respectively), suggesting a more efficient $T_1 \rightarrow S_1$ up-conversion arising from smaller ΔE_{ST} (Table 1). From the room-temperature fluorescence and the low-temperature phosphorescence (5 K) spectra of the doped films, the experimental ΔE_{ST} values are found to be in the order of Cz-VPN (0.36 eV) > Ac-VPN (0.20 eV) > Px-VPN (0.08 eV) ≈ Ac-CNP (0.09 eV) > Px-CNP (0.04 eV), which are in good agreement with the trend of the delayed emission lifetimes.

2.4. Electroluminescence Performance

Color-tunable TADF characteristics with high Φ_{PL} enable these emitters to be adopted in high-efficiency full-color TADF-OLEDs. To investigate the EL performance, multilayer OLEDs were fabricated using 6 wt%-emitter:host doped films as the emitting layer (EML). The structure of the fabricated devices was as follows: indium–tin-oxide (ITO, 110 nm)/α-NPD (40 nm)/mCP (10 nm)/EML (20 nm)/PPF (10 nm)/TPBi (30 nm)/LiF (0.8 nm)/Al (100 nm), where 4,4′-bis[*N*-(1-naphthyl)-*N*-phenylamino]-1,1′-biphenyl (α-NPD) and 1,3,5-tris(*N*-phenylbenzimizazol-2-yl)benzene (TPBi) served as a hole-transporting layer (HTL) and electron-transporting layer

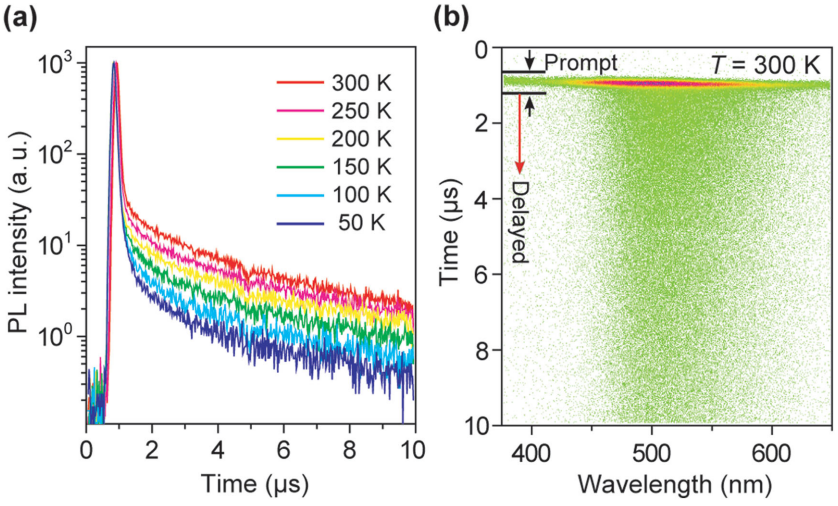

Figure 5. a) Temperature dependence of transient PL decay of a 6 wt%-Ac-VPN:mCBP doped film. b) Streak image of the doped film measured at 300 K under vacuum, in which green dots represent PL photon counts.

(ETL), respectively. To prevent the energy transfer and to confine T_1 excitons in the EML, thin layers of 1,3-bis(carbazol-9-yl) benzene (mCP) and PPF with high T_1 energies were inserted at the EML/HTL and EML/ETL interfaces. The current density–voltage–luminance (*J*–*V*–*L*) and η_{ext} versus luminance characteristics of the devices are shown in **Figure 6**, and the key device parameters are summarized in **Table 2**.

All the devices employing phthalonitrile and dicyanobenzene-based emitters displayed EL spectra similar to the corresponding PL spectra, confirming that EL emission was generated solely from the emitters via the same radiative decay process. These devices indicated similar turn-on voltages (V_{on}) in the range of 4.4–5.5 V. For the Cz-VPN-based device, a blue EL emission at a maximum wavelength (λ_{EL}) of 465 nm and Commission Internationale de l'Éclairage (CIE) color coordinates of (0.15, 0.18) were obtained. The EL efficiency of the blue-emitting Cz-VPN device is drastically decreased with increasing luminance. This severe efficiency roll-off of the device is mainly attributed to the relatively longer T_1 excited-state lifetime of the Cz-VPN emitter, which undergoes exciton quenching such as triplet–triplet annihilation and/or triplet–polaron annihilation.[16] Another possible reason can be the poor hole-transport property of the PPF host. PPF is a unipolar electron-transporting material and the hole/electron carrier balance is disrupted at high current densities. We anticipate that the performance and roll-off behavior of the blue TADF device can further be improved by using suitable bipolar hosts with high T_1 values and blue TADF emitters with shorter excited-state lifetimes.

High EL efficiencies with η_{ext} of 18.9%, 14.9%, and 13.3% are attained for the devices containing Ac-VPN, Px-VPN, and Ac-CNP, respectively (corresponding power efficiencies (η_p) are 34.1, 26.7, and 26.1 lm W^{-1}, respectively), and their EL emissions are located in the light-blue, green, and yellow regions, respectively. It is noteworthy that the Ac-VPN- and Px-VPN-based devices showed very small efficiency roll-off; hence, the η_{ext} of the devices were still high (12.4% and 10.4%, respectively), even at a high luminance of 10 000 cd m^{-2}. For the

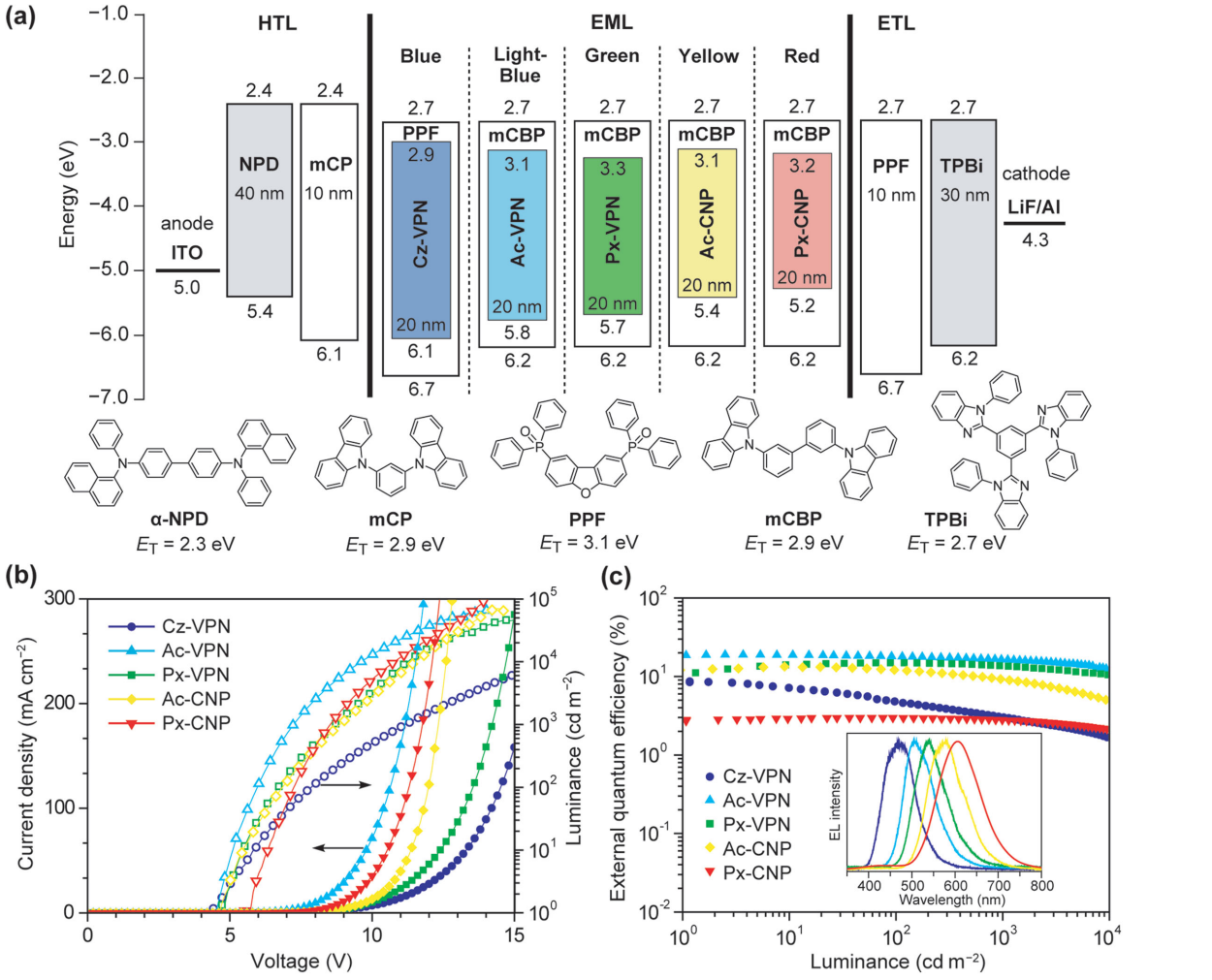

Figure 6. a) Energy level diagram and molecular structures of materials used for TADF-OLEDs. b) Current density–voltage–luminance (*J*–*V*–*L*) characteristics and c) external EL quantum efficiency (η_{ext}) versus luminance plots of the TADF-OLEDs. The inset of panel (c) represents normalized EL spectra of the devices measured at 10 mA cm^{-2}.

Table 2. EL performance of the TADF-OLEDs.

TADF emitter[a)]	Host	λ_{EL} [nm]	V_{on} [V]	L_{max} [cd m^{-2}]	η_{ext} [%]	η_c [cd A^{-1}]	η_p [lm W^{-1}]	CIE (x, y)
Cz-VPN	PPF	465	4.4	13,590	8.7	18.0	12.3	(0.15, 0.18)
Ac-VPN	mCBP	504	4.5	65,720	18.9	51.7	34.1	(0.23, 0.50)
Px-VPN	mCBP	537	4.7	44,380	14.9	45.4	26.7	(0.35, 0.57)
Ac-CNP	mCBP	580	4.7	70,630	13.3	38.1	26.1	(0.47, 0.51)
Px-CNP	mCBP	606	5.5	101,860	3.0	5.8	3.1	(0.53, 0.44)

[a)] λ_{EL}: EL emission maximum, V_{on}: turn-on voltage at 1 cd m^{-2}, L_{max}: maximum luminance, η_{ext}: maximum external EL quantum efficiency, η_c: maximum current efficiency, η_p: maximum power efficiency, CIE: Commission Internationale de l'Éclairage color coordinates measured at 10 mA cm^{-2}, PPF: 2,8-bis(diphenylphosphoryl)dibenzo[*b*,*d*]furan, mCBP: 3,3′-bis(carbazol-9-yl)-1,1′-biphenyl.

red-emitting Px-CNP-based device, the η_{ext} was inferior compared to those of the other devices because of the relatively lower Φ_{PL} of 15% in its doped film. However, the Px-CNP-based device exhibited only a slight efficiency roll-off owing to its short T_1 exciton lifetime of 1.5 µs, compared to other TADF emitters (Table 1).

Under electrical excitation in TADF-OLEDs, the T_1 excitons are directly generated by carrier recombination and are subsequently converted into the S_1 state via an efficient RISC. Accordingly, the theoretical maxima of η_{int} and η_{ext} can be given by the following equations[5a]

$$\eta_{int} = \eta_S \times \Phi_p + \eta_S \times \Phi_d + \eta_T \times \Phi_d / \Phi_{ISC} \quad (1)$$

$$\eta_{ext} = \eta_{int} \times \eta_{out} \quad (2)$$

where η_S and η_T denote the singlet-exciton and triplet-exciton production rates (25% and 75%, respectively), Φ_{ISC} is the intersystem-crossing efficiency ($\Phi_{ISC} = 1 - \Phi_p$), and η_{out} is the light out-coupling efficiency. The theoretical maxima of η_{ext} for Cz-VPN, Ac-VPN, Px-VPN, Ac-CNP, and Px-CNP-based devices are estimated to be ≈9%, 17%, 14%, 13%, and 3%, respectively, by assuming that η_{out} is ≈20%.[17] These theoretical values are consistent with the experimentally obtained η_{ext} values (Table 2), implying that the appropriate carrier balance and effective exciton confinement are indeed achieved in the EML for the full-color TADF-OLEDs.

3. Conclusion

A new series of full-color TADF emitters was designed and synthesized by combining a phthalonitrile or dicyanopyrazine acceptor core with various donor units. The photophysical properties of these materials could be tuned by a rational combination of the donor and acceptor constituents. The TADF emissions of the doped films depend on their HOMO–LUMO energy gap, and the emission occurred at wavelengths ranging from the blue (450 nm) to red (610 nm) region, spanning the entire visible region. Moreover, their small ΔE_{ST} originating from the angular-linked donor–acceptor structures induces efficient TADF characteristics. The OLEDs based on these emitters exhibited a high maximum external EL quantum efficiencies of up to 18.9% and an extremely small efficiency roll-off. We believe that these results open new avenues for designing high-performance full-color TADF emitters with simple and versatile structures for OLED applications.

4. Experimental Section

General Methods: NMR spectra were recorded on an Avance III 500 or Avance III 400 spectrometer (Bruker). Chemical shifts of ^{1}H and ^{13}C NMR signals were quoted to tetramethylsilane (δ = 0.00), $CDCl_3$ (δ = 77.0) as internal standards, respectively. Matrix-assisted laser desorption ionization time-of-flight mass spectra were collected on an Autoflex III spectrometer (Bruker Daltonics) using dithranol as the matrix. Elemental analyses were carried out with a Yanaco MT-5 CHN corder. UV–vis absorption and PL spectra were measured with a UV-2550 spectrometer (Shimadzu) and a Fluoromax-4 spectrophotometer (Horiba Scientific), respectively, using degassed spectral grade solvents. The PL quantum yields were measured using an integration sphere system C9920-02 coupled with a PMA-11 photonic multichannel analyzer (Hamamatsu Photonics). The transient PL measurements of doped thin films were performed using a C4334 Streak camera (Hamamatsu Photonics) with a N_2 gas laser (λ = 337 nm, pulse width = 500 ps, repetition rate = 20 Hz) under vacuum ($<4 \times 10^{-1}$ Pa). The HOMO energy levels of thin films were determined using an AC-3 ultraviolet photoelectron spectrometer (Riken-Keiki). The LUMO energy levels were estimated by subtracting the optical energy gap (E_g) from the measured HOMO energies; E_g values were determined from the onset position of the PL spectra of thin films. All quantum-chemical calculations were performed using the Gaussian 09 program package. Geometries in the ground state were optimized using the B3LYP functional with the 6–31G(d,p) basis set. Low-lying excited singlet and triplet states were computed using the optimized structures with TD-DFT at the same level.

Preparation of Materials: All regents and solvents for the synthesis were purchased from Sigma-Aldrich, Tokyo Chemical Industry, or Wako Pure Chemical Industries, and were used as received unless otherwise stated. 9,9-Dimethylacridan (Ac)[18] and PPF[13] were prepared according to the reported procedures. Other OLED materials were purchased from Luminescence Technology, Corp. The detailed synthetic procedures and characterization data of compounds **1**–**8** are described in the Supporting Information. All reactions were performed under nitrogen atmospheres in dry solvents. All final products were purified by temperature-gradient sublimation under vacuum before the measurements and device fabrication.

Synthesis of Cz-VPN: A mixture of **2** (1.65 g, 2.8 mmol), **3** (1.05 g, 5.8 mmol), bis(tri-*tert*-butylphosphine)palladium(0) (Pd(*t*-$Bu_3P)_2$, 0.03 g, 0.06 mmol), and potassium carbonate (2.28 g, 16.5 mmol) in dry toluene (30 mL) was refluxed for 48 h. After cooling to room temperature, the reaction mixture was filtered through a Celite pad, and the filtrate was concentrated under reduced pressure. The crude product was purified by column chromatography on silica gel (hexane/dichloromethane = 4:1, v/v)

to afford Cz-VPN as a white solid (yield = 1.85 g, 84%). ^{1}H NMR (500 MHz, $CDCl_3$, δ): 8.06 (t, J = 8.0 Hz, 2H), 7.97 (d, J = 7.4 Hz, 2H), 7.39–7.26 (m, 12H), 7.19–7.01 (m, 12H), 6.89 (t, J = 7.0 Hz, 2H), 6.73–6.61 (m, 2H), 1.70 (s, 6H); ^{13}C NMR (125 MHz, $CDCl_3$, δ): 146.54, 139.44, 138.95, 137.26, 136.02, 131.32, 129.81, 128.90, 128.86, 128.73, 128.56, 126.35, 123.99, 121.09, 120.06, 120.03, 118.16, 115.19, 109.60, 109.11, 19.92; MS (MALDI-TOF) m/z: $[M]^+$ calcd 790.31; found, 790.56. Anal. calcd for $C_{58}H_{38}N_4$: C 88.07, H 4.84, N 7.08; found: C 88.16, H 4.74, N 7.07.

Synthesis of Ac-VPN: A mixture of 4,5-dichlorophthalonitrile (0.99 g, 5.0 mmol), **5** (4.17 g, 10.1 mmol), tetrakis(triphenylphosphine) palladium(0) ($Pd(PPh_3)_4$, 0.06 g 0.05 mmol), potassium iodide (1.66 g, 10.0 mmol), and potassium phosphate (4.31 g, 20.0 mmol) in dry 1,4-dioxane (10 mL) was refluxed for 48 h. After cooling to room temperature, the reaction mixture was added into water and was extracted with dichloromethane. The combined organic layers were washed with water and dried over anhydrous magnesium sulfate. After filtration and evaporation, the crude product was purified by column chromatography on silica gel (hexane/dichloromethane = 4:1, v/v) to give Ac-VPN as a yellow solid (yield = 1.18 g, 34%). ^{1}H NMR (500 MHz, $CDCl_3$, δ): 7.99 (s, 1H), 7.95 (s, 1H), 7.69 (d, J = 8.5 Hz, 4H), 7.49 (td, J = 7.5 Hz, 1.5 Hz, 8H), 7.03–6.94 (m, 8H), 6.30 (dd, J = 8.0 Hz, 1.5 Hz, 4H), 1.53 (s, 12H); ^{13}C NMR (125 MHz, $CDCl_3$, δ): 145.39, 142.84, 140.58, 138.43, 135.87, 135.25, 135.09, 131.81, 131.55, 130.41, 126.42, 125.39, 121.02, 115.78, 114.54, 114.01, 36.04, 31.15; MS (MALDI-TOF) m/z: $[M+H]^+$ calcd 695.32; found, 695.71. Anal. calcd for $C_{50}H_{38}N_4$: C 86.42, H 5.51, N 8.06; found: C 86.32, H 5.48, N 7.99.

Synthesis of Px-VPN: Px-VPN was synthesized according to the same procedure as described above for the synthesis of Ac-VPN, except that **7** (3.91 g, 10.1 mmol) was used as the reactant instead of **5**, yielding an orange solid (yield = 0.98 g, 31%). ^{1}H NMR (500 MHz, $CDCl_3$, δ): 8.01 (s, 2H), 7.39 (d, J = 8.0 Hz, 4H), 7.33 (d, J = 8.0 Hz, 4H), 6.69 (d, J = 7.8 Hz, 4H), 6.65–6.54 (m, 4H), 6.48 (t, J = 7.4 Hz, 4H), 5.82 (d, J = 7.4 Hz, 4H); ^{13}C NMR (125 MHz, $CDCl_3$, δ): 145.15, 143.92, 139.87, 137.60, 135.17, 133.77, 132.13, 131.32, 123.41, 121.76, 115.69, 115.24, 115.06, 112.93; MS (MALDI-TOF) m/z: $[M]^+$ calcd 642.21; found, 642.35. Anal. calcd for $C_{44}H_{26}N_4O_2$: C 82.23, H 4.08, N 8.72; found: C 82.23, H 3.99, N 8.77.

Synthesis of Ac-CNP: A mixture of **8** (1.01 g, 2.3 mmol), 9,9-dimethylacridan (1.05 g, 5.0 mmol), bis(tri-*tert*-butylphosphine) palladium(0) ($Pd(t\text{-}Bu_3P)_2$, 0.12 g, 0.23 mmol), and potassium carbonate (0.95 g, 6.9 mmol) in dry toluene (30 mL) was refluxed for 72 h. After cooling to room temperature, the reaction mixture was filtered through a Celite pad, and the filtrate was concentrated under reduced pressure. The crude product was purified by column chromatography on silica gel (hexane/ethyl acetate = 5:1, v/v) to afford Ac-CNP as an orange solid (yield = 0.64 g, 40%). ^{1}H NMR (500 MHz, $CDCl_3$, δ): 7.86 (d, J = 8.5 Hz, 4H), 7.47–7.43 (m, 8H), 6.97–6.90 (m, 8H), 6.35 (dd, J = 7.8 Hz, 1.5 Hz, 4H), 1.66 (s, 12H); ^{13}C NMR (125 MHz, $CDCl_3$, δ): 154.77, 144.69, 140.35, 134.21, 132.33, 131.42, 130.84, 130.16, 126.47, 125.28, 121.48, 114.64, 113.04, 36.18, 30.66; MS (MALDI-TOF) m/z: $[M]^+$ calcd 696.30; found, 696.49. Anal. calcd for $C_{48}H_{36}N_6$: C 82.73, H 5.21, N 12.06; found: C 82.21, H 5.16, N 11.85.

Synthesis of Px-CNP: Px-CNP was synthesized according to the same procedure as described above for the synthesis of Ac-CNP, except that phenoxazine (0.92 g, 5.0 mmol) was used as the reactant instead of 9,9-dimethylacridan, yielding a red solid (yield = 1.03 g, 69%). ^{1}H NMR (500 MHz, $CDCl_3$, δ): 7.81 (d, J = 8.6 Hz, 4H), 7.45 (d, J = 8.6 Hz, 4H), 6.72 (dd, J = 8.0 Hz, 1.6 Hz, 4H), 6.68 (td, J = 7.6 Hz, 1.4 Hz, 4H), 6.57 (td, J = 7.6 Hz, 1.6 Hz, 4H), 5.96 (dd, J = 8.0 Hz, 1.4 Hz, 4H); ^{13}C NMR (125 MHz, $CDCl_3$, δ): 154.53, 144.13, 142.36, 134.79, 133.42, 132.49, 131.34, 130.30, 123.39, 122.13, 115.90, 113.23, 112.92; MS (MALDI-TOF) m/z: $[M]^+$ calcd 644.20; found, 644.43. Anal. calcd for $C_{42}H_{24}N_6O_2$: C 78.25, H 3.75, N 13.04; found: C 78.33, H 3.65, N 13.13.

Device Fabrication and Measurements: ITO-coated glass substrates were cleansed with detergent, deionized water, acetone, and isopropanol. The substrates were then subjected to UV–ozone treatment for 15 min, before loading them into a vacuum evaporation system. The organic layers were thermally evaporated on the substrates under vacuum ($<3 \times 10^{-4}$ Pa) with an evaporation rate of <0.3 nm s^{-1}. A cathode aluminum layer was then deposited through a shadow mask. The layer thickness and the deposition rate were monitored in situ during deposition by an oscillating quartz thickness monitor. The current density–voltage–luminance characteristics of the devices were measured using an E5273A semiconductor parameter analyzer (Agilent) and a 1930-C optical power meter (Newport). The EL spectra were recorded using an SD2000 multi-channel analyzer (Ocean Optics).

Supporting Information

Supporting Information is available from the Wiley Online Library or from the author.

Acknowledgements

This work was partially supported by the ACCEL project from Japan Science and Technology Agency (JST), and Grants-in-Aid for Scientific Research on Innovative Areas "3D Active-Site Science" (Grant No. 15H01049), Young Scientists (A) (Grant No. 25708032), and Challenging Exploratory Research (Grant No. 26620168) from Japan Society for the Promotion of Science (JSPS), the Cooperative Research Program of "Network Joint Research Center for Materials and Devices," the Casio Science Promotion Foundation, the Ogasawara Foundation for the Promotion of Science and Engineering, and the Kurata Memorial Hitachi Science and Technology Foundation.

Received: November 28, 2015
Revised: January 6, 2016
Published online: February 12, 2016

[1] a) C. W. Tang, S. A. VanSlyke, *Appl. Phys. Lett.* **1987**, *51*, 913; b) J. Kido, M. Kimura, K. Nagai, *Science* **1995**, *267*, 1332; c) S. Reineke, F. Lindner, G. Schwartz, N. Seidler, K. Walzer, B. Lüssem, K. Leo, *Nature* **2009**, *459*, 234; d) M. A. McCarthy, B. Liu, E. P. Donghue, I. Kravchenko, D. Y. Kim, F. So, A. G. Rinzler, *Science* **2011**, *332*, 570.

[2] M. A. Baldo, D. F. O'Brien, Y. You, A. Shoustikov, S. Sibley, M. E. Thompson, S. R. Forrest, *Nature* **1998**, *395*, 151.

[3] a) C. Adachi, M. A. Baldo, M. A. Thompson, S. R. Forrest, *J. Appl. Phys.* **2001**, *90*, 5048; b) C. Adachi, M. A. Baldo, S. R. Forrest, M. E. Thompson, *Appl. Phys. Lett.* **2000**, *77*, 904.

[4] a) H. Uoyama, K. Goushi, H. Nomura, C. Adachi, *Nature* **2012**, *492*, 234; b) T. Nishimoto, T. Yasuda, S. Y. Lee, R. Kondo, C. Adachi, *Mater. Horiz.* **2014**, *1*, 264; c) Y. J. Cho, K. S. Yook, J. Y. Lee, *Sci. Rep.* **2015**, *5*, 7859; d) Y. J. Cho, B. D. Chin, S. K. Jeon, J. Y. Lee, *Adv. Mater.* **2015**, *25*, 6786; e) Y. J. Cho, S. K. Jeon, B. D. Chin, E. Yu, J. Y. Lee, *Angew. Chem. Int. Ed.* **2015**, *54*, 5201; f) S. Wang, X. Yan, Z. Cheng, H. Zhang, Y. Liu, Y. Wang, *Angew. Chem. Int. Ed.* **2015**, *54*, 13068.

[5] a) S. Y. Lee, T. Yasuda, H. Nomura, C. Adachi, *Appl. Phys. Lett.* **2012**, *101*, 093306; b) A. Endo, K. Sato, K. Yoshimura, T. Kai, A. Kawada, H. Miyazaki, C. Adachi, *Appl. Phys. Lett.* **2011**, *98*, 083302; c) K. Sato, K. Shizu, K. Yoshimura, A. Kawada, H. Miyazaki, C. Adachi, *Phys. Rev. Lett.* **2013**, *110*, 247401; d) H. Tanaka, K. Shizu, H. Miyazaki, C. Adachi, *Chem. Commun.* **2012**, *48*, 11392; e) S. Hirata, Y. Sakai, K. Masui, H. Tanaka, S. Y. Lee, H. Nomura, N. Nakamura, M. Yasumatsu, H. Nakanotani, Q. Zhang, K. Shizu, H. Miyazaki, C. Adachi, *Nat. Mater.* **2015**, *14*, 330; f) M. Kim, S. K. Jeon, S.-H. Hwang, J. Y. Lee, *Adv. Mater.* **2015**, *27*, 2515; g) D. Y. Lee,

M. Kim, S. K. Jeon, S.-H. Hwang, C. W. Lee, J. Y. Lee, *Adv. Mater.* **2015**, *27*, 5861; h) W.-L. Tsai, M.-H. Huang, W.-K. Lee, Y.-J. Hsu, K.-C. Pan, Y.-H. Huang, H.-C. Ting, M. Sarma, Y.-Y. Ho, H.-C. Hu, C.-C. Chen, M.-T. Lee, K.-T. Wong, C.-C. Wu, *Chem. Commun.* **2015**, *51*, 13662; i) J. W. Sun, J. Y. Baek, K.-H. Kim, C.-K. Moon, J.-H. Lee, S.-K. Kwon, Y.-H. Kim, J.-J. Kim, *Chem. Mater.* **2015**, *27*, 6675.

[6] a) Q. Zhang, J. Li, K. Shizu, S. Huang, S. Hirata, H. Miyazaki, C. Adachi, *J. Am. Chem. Soc.* **2012**, *134*, 14706; b) Q. Zhang, B. Li, S. Huang, H. Nomura, H. Tanaka, C. Adachi, *Nat. Photonics* **2014**, *8*, 326; c) F. B. Dias, K. N. Bourdakos, V. Jankus, K. C. Moss, K. T. Kamtekar, V. Bhalla, J. Santos, M. R. Bryce, A. P. Monkman, *Adv. Mater.* **2013**, *25*, 3707; d) H. Wang, L. Xie, Q. Peng, L. Meng, Y. Wang, Y. Yi, P. Wang, *Adv. Mater.* **2014**, *26*, 5198; e) Z. Xie, C. Chen, S. Xu, J. Li, Y. Zhang, S. Liu, J. Xu, Z. Chi, *Angew. Chem. Int. Ed.* **2015**, *54*, 7181.

[7] a) S. Y. Lee, T. Yasuda, Y. S. Yang, Q. Zhang, C. Adachi, *Angew. Chem. Int. Ed.* **2014**, *126*, 6520; b) S. Y. Lee, T. Yasuda, I. S. Park, C. Adachi, *Dalton Trans.* **2015**, *44*, 8356; c) Q. Zhang, D. Tsang, H. Kuwabara, Y. Hatae, B. Li, T. Takahashi, S. Y. Lee, T. Yasuda, C. Adachi, *Adv. Mater.* **2015**, *27*, 2096.

[8] a) G. Méhes, H. Nomura, Q. Zhang, T. Nakagawa, C. Adachi, *Angew. Chem. Int. Ed.* **2012**, *51*, 11311; b) K. Nasu, T. Nakagawa, H. Nomura, C.-J. Lin, C.-H. Cheng, M.-R. Tseng, T. Yasuda, C. Adachi, *Chem. Commun.* **2013**, *49*, 10385; c) H. Ohkuma, T. Nakagawa, K. Shizu, T. Yasuda, C. Adachi, *Chem. Lett.* **2014**, *43*, 1017.

[9] a) M. Numata, T. Yasuda, C. Adachi, *Chem. Commun.* **2015**, *51*, 9443; b) K. Suzuki, S. Kubo, K. Shizu, T. Fukushima, A. Wakamiya, Y. Murata, C. Adachi, H. Kaji, *Angew. Chem. Int. Ed.* **2015**, *54*, 15231; c) I. S. Park, M. Numata, C. Adachi, T. Yasuda, *Bull. Chem. Soc. Jpn.* **2016**, *89*, 10.1246/bcsj.20150399.

[10] a) N. J. Turro, V. Ramamurthy, J. C. Scaiano, *Modern Molecular Photochemistry of Organic Molecules*, University Science Books, Sausalito **2010**; b) Y. Tao, K. Tuan, T. Chen, P. Xu, H. Li, R. Chen, C. Zheng, L. Zhang, W. Huang, *Adv. Mater.* **2014**, *26*, 7931.

[11] a) J. W. Sun, J.-H. Lee, C.-K. Moon, K.-H. Kim, H. Shin, J.-J. Kim, *Adv. Mater.* **2014**, *26*, 5684; b) D. Y. Lee, B. S. Kim, C. W. Lee, Y. Im, K. S. Yook, S.-H. Hwang, J. Y. Lee, *ACS Appl. Mater. Interfaces* **2015**, *7*, 9625.

[12] R. F. Doering, R. S. Miner Jr., L. Rothman, E. I. Becker, *J. Org. Chem.* **1958**, *23*, 520.

[13] P. A. Vecchi, A. B. Padmaperuma, H. Qiao, J. S. Sapochak, P. E. Burrows, *Org. Lett.* **2006**, *8*, 4211.

[14] S. Gong, X. He, Y. Chen, Z. Jiang, C. Zhong, D. Ma, J. Qin, C. Yang, *J. Mater. Chem.* **2012**, *22*, 2894.

[15] a) J. V. Caspar, E. M. Kober, B. P. Sullivan, T. J. Meyer, *J. Am. Chem. Soc.* **1982**, *104*, 630; b) S. D. Cummings, R. Eisenberg, *J. Am. Chem. Soc.* **1996**, *118*, 1949.

[16] a) C. Murawski, K. Leo, M. C. Gather, *Adv. Mater.* **2013**, *25*, 6801; b) Y. Zhang, S. R. Forrest, *Phys. Rev. Lett.* **2012**, *108*, 267404; c) M. A. Baldo, C. Adachi, S. R. Forrest, *Phys. Rev. B: Condens. Matter* **2000**, *62*, 10967; d) K. Masui, H. Nakanotani, C. Adachi, *Org. Electron.* **2013**, *14*, 2721.

[17] a) B. E. A. Saleh, M. C. Teich, *Fundamentals of Photonics*, Wiley, New York **1991**; b) S. Nowy, B. C. Krummacher, J. Frischeisen, N. A. Reinke, W. Brütting, *J. Appl. Phys.* **2008**, *104*, 123109; c) J.-S. Kim, P. K. H. Ho, N. C. Greenham, R. H. Friend, *J. Appl. Phys.* **2000**, *88*, 1073.

[18] T. Takahashi, K. Shizu, T. Yasuda, K. Togashi, C. Adachi, *Sci. Technol. Adv. Mater.* **2014**, *15*, 034202.